Journal of Cancer Biomoleculars and Therapeutics

ETERNO PRESS

Article

Camptothecin and its Analogues as Putative Bruton Tyrosine Kinase (BTK) Inhibitors in Cancer Therapy - Biophysical Simulations of Wild Type and C481S Mutation

Abdul Rashid Issahaku, Mahmoud E.S Soliman*

Molecular Bio-computation and Drug Design Laboratory, School of Health Sciences, University of KwaZulu-Natal, Westville Campus, Durban 4001, South Africa.

*Corresponding Author: Mahmoud E.S. Soliman, soliman@ukzn.ac.za

Article history

Received: 23 May 2024
Revised: 30 June 2024
Accepted: 4 July 2024
Published online: 7 July 2024

Keywords

Camptothecin
Natural Anticancer
Chinese Traditional Medicine
Drug Repurposing
Bruton's Tyrosine Kinase

Abstract

Camptothecin (CPT) and its derivatives are extracted from the Chinese tree *Camptotheca acuminata* and have been long known for their significant antitumor activity. The widely reported primary mechanism of their anti-cancer activity is through inhibition of topoisomerase I (Topo I), a key anticancer target. However, there is a lack of research on other possible mechanisms of action of CPT and its analogues (CPT/analogues). In this report, we investigated the potential inhibitory mechanism of CPT/derivatives against Bruton's tyrosine kinase (BTK) – a crucial protein for regulating various cellular functions and is essential for B-cell growth and cyclical division. The binding mechanism of CPT and its analogues (Irinotecan, Diflomotecan, and Topotecan) against BTK was investigated using molecular docking, molecular dynamics simulations and thermodynamic binding free energy calculations. NRX-0492, a potent orally active degrader of both wild-type and mutant BTK, was used as a reference/control inhibitor. We also included a set of active binders (actives) and non-binders (inactives) to distinguish between effective binders and false positives to ensure the validity of our results. Binding affinity analysis suggested that CPT and its analogues could potentially bind to BTK comparably to NRX-0492. The studied compounds demonstrated stable binding with the protein throughout the simulation time via hydrogen bonds, π-π interactions, van der Waals forces and π-sulfur interactions. Irinotecan exhibited a binding affinity of $\Delta G_{binding}$ = –42.4±5.3 kcal/mol, closely matching that of NRX-0492 ($\Delta G_{binding}$ = –48.8±3.4 kcal/mol). Furthermore, the activity of CPT/derivatives was examined against the C481S mutant. Although the activity was slightly decreased due to the mutation, the compounds retained a promising binding affinity when compared to the results of NRX-0492. The findings of this study provide foundation for future experimental investigation of unexplored potential anti-cancer mechanism of CPT/derivatives and offer a new perspective on repurposing of natural products in cancer therapy.

Graphical Abstract

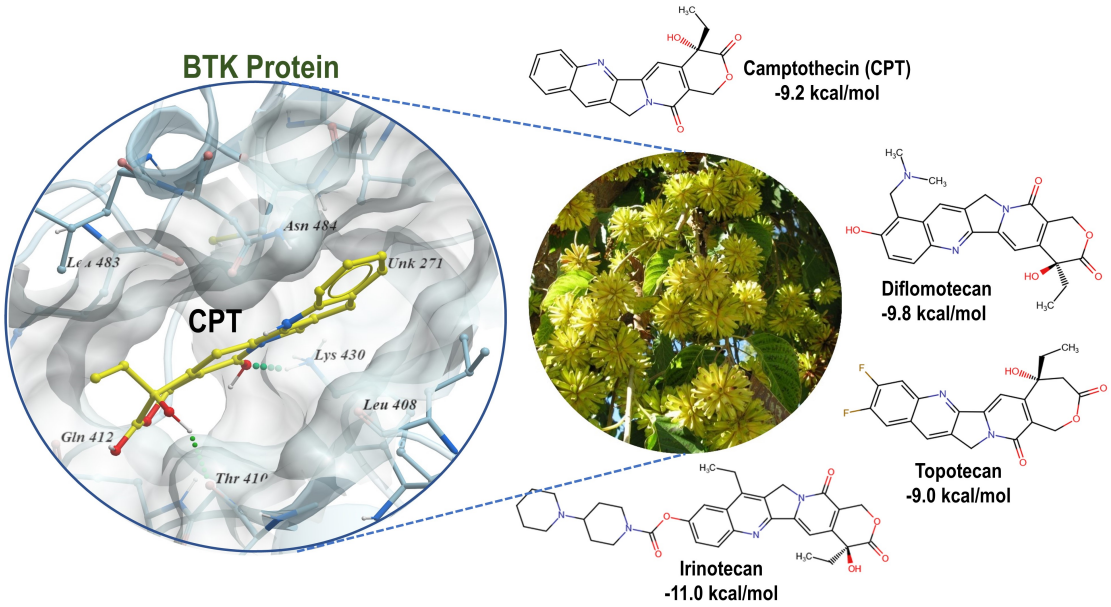

1. Introduction

Natural products have gained popularity as a source of bioactive small molecules, which make up 90% of pharmaceutical drugs, due to their low cost and enhanced safety profile [1]. Moreover, they provide an abundance of structural diversity which is crucial feature for discovery of effective therapeutics compared to conventional synthetic molecules [1].

Camptothecin (CPT) was discovered in crude extracts over 60 years ago, but only two CPT analogues, Irinotecan and Topotecan, have been approved for cancer treatment despite the synthesis of large number of analogues over the past six decades [2]. Clinical trials for CPT in cancer patients, including Phase I and Phase II [3,4] were conducted in the United States. CPT was used clinically in China until the mid-1970s for treating stomach and bladder cancer and certain phenotypes of leukemia, often in combination with corticosteroids [3,5]. The pharmacokinetic profile and ADME properties of CPT and its derivatives have been thoroughly investigated in previous studies [6].

CPT and its analogues have been reported to target human DNA topoisomerase I (Topo I) by preventing the rejoining step in the Topo I cleavage/relegation reaction, leading to the accumulation of a covalent reaction intermediate [7]. This was long known to be the primary mechanism of the anti-cancer activity of CPT and its derivatives. Research on other potential mechanisms of the anticancer activity of CPT and its analogues is lacking in literature. Although several reports discussed the mechanism of action of CPT and its analogues, yet, the main emphasis of their antitumor activity is attributed to binding with Topo I [2,7,8]

Despite the conclusion of CPT clinical trials in the 1970s, research efforts have continued to explore other possible mechanisms [9-11]. A novel mechanism of action was reported in 2021 showing that CPT inhibits neddylation and induces upregulation of p-IkBa, thereby blocking the NF-κB pathway [12]. Given the crucial role of Topo I in genetic transcription control [13], it is important to explore whether CPT or its analogues can modulate gene expression independently of Topo I inhibition. Mabb *et al.* in 2016 reported certain CPTs are capable of modulating gene expression independent of Topo I function [14]. Another study by Li *et al.* [2] has argued that Topo I may not be the optimal target for cancer therapeutics, and developed a series of novel CPT derivatives that target other possible targets than Topo I [2]. The current work is an additional attempt to comprehend and investigate potential mechanisms of action for the anti-cancer activity of CPT and its derivatives.

The man aim of this report is to investigate whether Bruton's tyrosine kinase (BTK) could be a potential target for CPT/analogues and provide insight into the nature of such unexplored mechanism of action. The rationale behind considering BTK specifically for this investigation than other cancer targets was based on the following rational.

Protein kinases are enzymes that facilitate the phosphorylation of proteins, altering their function or interactions with other proteins [15]. Dysregulation of kinase activity can lead to hallmark features of cancer, such as changes in cellular proliferation, motility, metabolism, angiogenesis, survival, and the circumvention of antitumor immune responses [16,17]. Bruton's tyrosine kinase (BTK) is a member of the kinase family, playing a pivotal role in oncogenic signaling essential for the survival of leukemic cells in various B-cell phenotypic malignancies [18]. BTK is also involved in downstream signaling pathways of several receptors, including Toll-like receptors (TLRs) and G protein-coupled chemokine receptors [19,20]. This underscores its importance as a strategic target for cancer therapy.

Mutations in BTK signaling are implicated in the etiology and perpetuation of B-cell lymphomas and autoimmune diseases [21,22]. As a result, small molecule inhibitors targeting BTK have emerged as a promising therapeutic approach for autoimmune diseases and hematologic malignancies. Several research efforts have led to the development of several BTK inhibitors, with three compounds approved by the U.S. Food and Drug Administration (FDA): ibrutinib (2013), acalabrutinib (2017), and zanubrutinib (2020) [23-25], while others are in various stages of clinical trials [26-31] (Figure 1). Despite these advancements, synthetic drugs often come with side effects, prompting a shift in focus towards natural compounds as effective and safer therapeutics.

Furthermore, it was reported that CPT exhibits its most cytotoxic activity during the S-phase of the cell cycle. However, subsequent research found that CPT also inhibits cellular cycle progression at both the S and G2 stages [32]. Additionally, it has been reported that BTK-deficient B-cells enter early in the G1 stage but do not progress to the S stage of the cellular cycle due to a failure to induce cyclin D2 expression. Putting all above-mentioned facts together, we propose a novel mechanism of the anti-cancer activity of CPT and its analogs as potential BTK inhibitors. CPT and its analogues, Irinotecan, Diflomotecan, and Topotecan were investigated in this study. To rationally assess the potential inhibitory activity of CPT and its analogues against BTK, NRX-0492, an orally active and potent degrader of wild-type and mutant BTK [33], was included as a control/reference drug. Moreover, a set of binders and non-binders were included to ensure that our simulation protocols produce valid and reliable results. Additionally, the activity of CPT/derivatives was examined against the C481S mutant to see if CPT/derivatives may be effective against BTK mutations associated with resistance to noncovalent BTK inhibitors [34,35]. For this, several in silico approaches including molecular docking, molecular dynamics (MD) simulations, and thermodynamic binding free energy calculations were employed in this study.

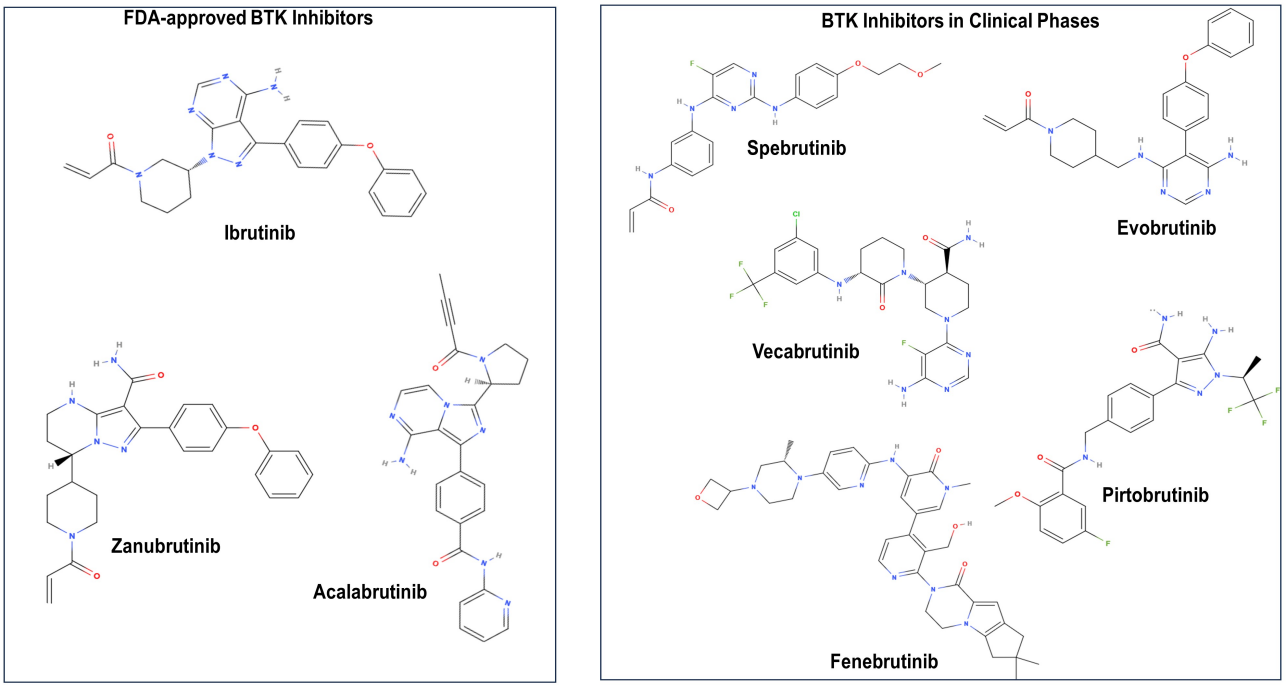

Figure 1. 2D structures of currently FDA-approved BTK inhibitors (left-hand panel) and BTK inhibitors in clinical phases (right-hand panel).

Findings of this report would serve as a solid starting point for further experimental investigations and creating new opportunities for repurposing medications against new biological targets for cancer therapy.

2. Methodology

2.1 BTK Preparation

The structure of the wild-type (WT) BTK in complex with NRX-0492 (PDB ID: 8EJB, resolution: 1.58 Å) and C481 mutant (PDB ID: 8FLN, resolution: 1.33 Å) were retrieved from the Protein Data Bank (https://www.rcsb.org/). These structures showed high resolution, hence chosen for this investigation. UCSF Chimera [36] was used to prepare the protein by removing all non-standard residues, including co-crystallized water molecules and heteroatoms. Hydrogen atoms were added based on the pKa calculations using H++ server (http://newbiophysics.cs.vt.edu/H++/) at pH of 7.0.

2.2 Preparation of CPT and its Analogues

The 2D structures of the CPT and its analogues were created using Marvin Sketch version 18.10.0 [37], and the structures were saved as MOL2 format for energy minimization using the Avogadro version 1.2.0 [38] using the united forcefield (UFF) with conjugate gradient algorithm for 200 steps with a specified energy difference cutoff of no more than 0.1.

2.3 Molecular Docking and Validation

PyRx graphical user interface [39] was used to prepare and analyze molecular docking simulations. AutoDock Vina software was employed as docking algorithm [40]. The binding site of BTK was determined based on the 3D structure of co-crystalized inhibitor (PDB ID: 8EJB) the with a grid box size of 25 Å × 21 Å × 20 Å, centered at x = 12.6074, y = –5.72388, and z = –14.1572. A designated exhaustiveness value of 8 and the specified parameters were saved in a configuration file for execution. To assess the validity and reliability of the docking protocol, we re-docked the co-crystalized NRX-0492 into the BTK binding site, and the docked structure was assessed by calculating the Root of Mean Square Deviation (RMSD) of the docked complex against experimentally determined X-ray structure. Furthermore, a set of experimentally known BTK binders (inhibitors) and non-binders were obtained from the Binding Database (https://www.bindingdb.org/) and included in the calculations to validate our binding affinity estimations.

2.4 Molecular Dynamics and Thermodynamic Calculations

Molecular dynamics (MD) simulations were performed using the GPU-based Particle Mesh Ewald Molecular Dynamics (PMEMD) version of AMBER 18 software [41]. AMBER force field of 14SB [42] was used to parameterize the protein, while General Amber Forcefield (GAFF) [43] was applied to the investigated ligands. The LEAP module was then used to add hydrogens and heavy atoms to the protein [41], and the Restrained Electrostatic Potential (RESP) approach was employed using the ANTECHAMBER module to assign atomic partial charges to the ligands [44]. The systems were solvated in a Transferable Intermolecular Potential with 3 Points (TIP3P) water box with an 8.0 Å buffer, and Na^+ and Cl- counter ions were added to

neutralize them. Van der Waals and long-range electrostatic interactions were managed using the Particle Mesh Ewald algorithm [45]. Energy minimization was conducted in two stages: the first 1000 steps using steep descent with restraints, followed by another 1000 steps using the conjugate gradient algorithm without restraints. The systems were then heated from 0 to 310 K in steps, applying a 5 kcal/mol Å² harmonic restraint potential within the NTP ensemble, utilizing a Langevin thermostat [46] with a collision frequency of 1.0 ps^{-1}. Subsequently, equilibration was performed at 310 K for 5 ns with restraints, maintaining a pressure of 1 bar using the Berendsen barostat [47]. SHAKE algorithm [48] was then employed to restrain all hydrogen bonds. Molecular dynamics production runs of 150 ns were then carried out for each system. The coordinates and trajectories generated from the simulation were analysed using the CPPTRAJ and PTRAJ modules [49] incorporated in the AMBER 18 program. Various molecular modelling tools such Discovery studio version v19.10.18289 and UCSF Chimera were used for visualization and analysis of the data. Origin data version 9.1 was used to create graphical plots of the created data [49].

2.5 Binding Energy Calculations

The binding free energies of the studied compounds against BTK were estimated using the Molecular Mechanics/Poisson-Boltzmann Area (MM/PBSA) approach [49]. These energies were averaged over 150 ns MD trajectory. The binding energies were calculated according to the following equations:

$$\Delta G_{binding} = G_{complex} - (G_{protein} + G_{ligand})$$

$$\Delta G_{binding} = E_{MM} + G_{solv} - T\Delta S$$

Where $\Delta G_{binding}$ indicates the total free energy of binding minus conformational entropy of binding ($T\Delta S$).

$$\Delta E_{MM} = \Delta E_{int} + \Delta E_{ele} + \Delta E_{vdW}$$

Where ΔE_{MM} denotes the total gas-phase energy, comprising internal energy, electrostatic, and van der Waals energy components. Internal energy encompasses the energy derived from various bonds, angles, and torsion.

$$E_{int} = E_{bond} + E_{angle} + E_{torsion}$$

The combination of polar ΔG_{PB} and non-polar ΔG_{SA} contributions to solvation are also represented as follows:

$$\Delta G_{solv} = \Delta G_{PG} + \Delta G_{SA}$$

G_{SA} was calculated based on the solvent accessible surface area (SASA) using a 1.4 Å water probe radius.

3. Results and Discussion

3.1 BTK PDB Structure Selection and Validation

The retrieved BTK protein structure was validated using PROCHECK server (https://www.ebi.ac.uk/thornton-srv/software/PROCHECK/), and the results are provided as Supplementary Material (Figure S1). The analysis indicated that 233 non-glycine and non-proline residues, representing 95.5%, fell within the most favored region, while 11 residues, representing 4.5%, fell within the additionally allowed region. A structure is considered good quality if over 90% of the residues lay within the favored region, indicating the structure is of high quality for further simulations [50]. To further ascertain the quality of the structure, the Quality Model Energy Analysis module (QMEAN) incorporated in the Swiss-Model online server was utilized. Analysis of the structure presented global QMEAN values of 0.86±0.05, which fell within the desired range (0-1) [50]. These favorable results further reposed confidence in the protein structure used for the study.

3.2 Docking Protocol and Validation of Docking Results

To assess the quality of the docking protocol in estimating the binding poses and affinities, we re-docked the co-crystalized NRX-0492 into the BTK binding site, and the docked structure was assessed by calculating the Root of Mean Square Deviation (RMSD) of the docked complex against experimentally determined X-ray structure. The RMSD value of 1.01 Å (Figure 2) is a good indication of valid docking protocol [51].

Moreover**,** to enrich the docking calculations and to ensure that we eliminate false positives or docking artifacts, we included experimentally determined active BTK inhibitors (binders) and inactive compounds (non-binder) form the binding database (www.bindingdb.org). Generally, binders and non-binders are selected based on an inhibitory concentration (IC_{50}) or inhibition constant (k_i), being ≤ 100 nM is considered a binder, and > 100 nM is considered a non-binder, according to a widely used scheme [52-54]. In this study, along with the reference drug NRX-0492, we included additional two binders (PubChem CID 91801213; k_i = 0.146 nM, and PubChem CID 25154877, k_i = 0.25 nM) and two non-binder compounds (PubChem CID16722836, k_i = 850 nM, and PubChem CID 72695751, k_i = 550 nM) (Figure 3).

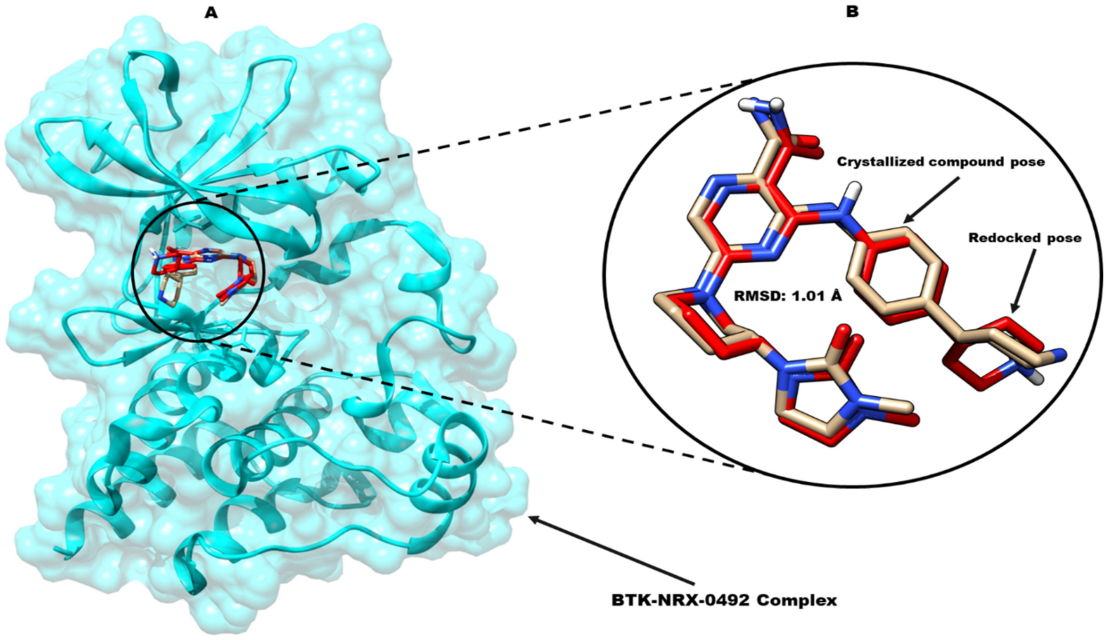

Figure 2. Validation of the docking protocol by re-docking the co-crystalized NRX-0492 into BTK binding site. (A) Superimposed structures of the docked NRX-0492 (red) and co-crystallized structure (light brown). (B) A close-up view of the superimposed structures.

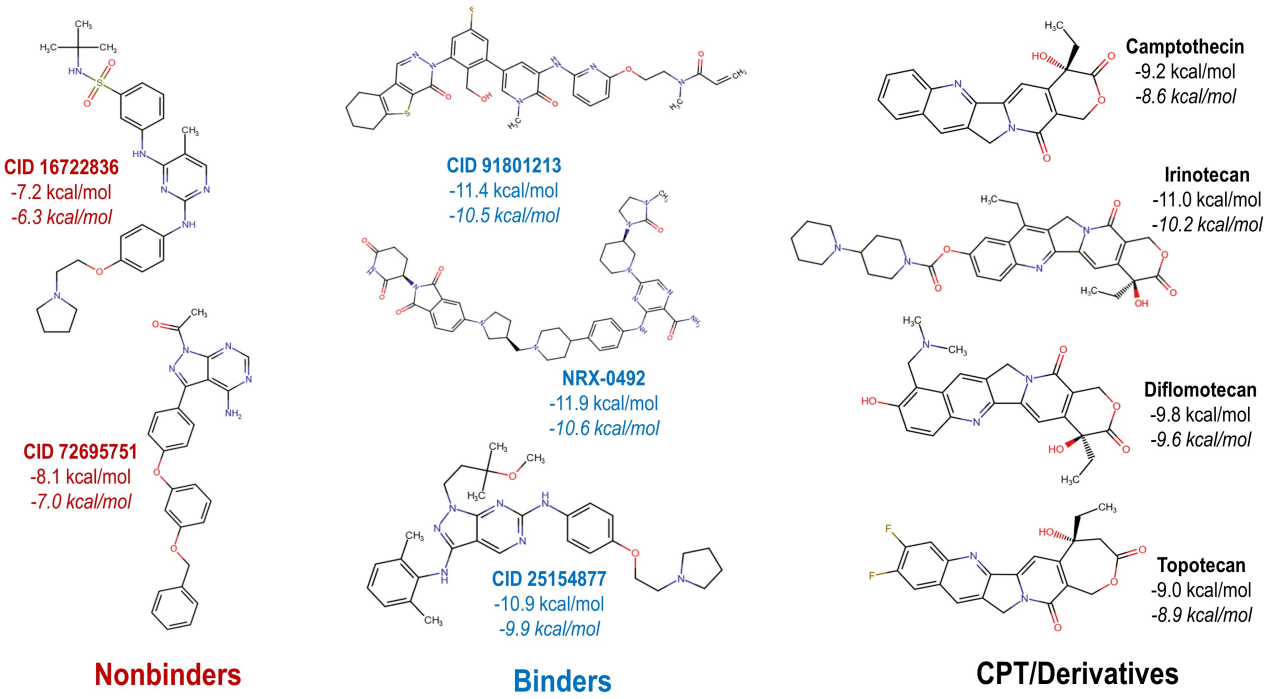

Figure 3. 2D chemical structures and the docking scores of CPT/analogues, NRX-0492, binders and non-binders against WT BTK and C481S mutant (*italic*).

3.3 Docking Results

The molecular docking binding scores are presented in Figure 3 and Table 1. The reference inhibitor NRX-0492 showed the highest binding affinity with a value of –11.9 kcal/mol, while CPT/derivatives exhibited promising docking scores with Irinotecan being the closest to the activity of the reference drug with binding energy of –11.0 kcal/mol. CPT, Diflomotecan and Topotecan exhibited lower binding affinity than NRX-0492 with binding energy of –9.2, –9.8 and –9.0, respectively.

C481S mutation resulted in overall decrease in the binding affinity across all studied compounds, however, it was interesting to notice that C481S mutation had less negative effect on the binding CPT/derivatives than

NRX-0492 (Figure 3 and Table 1), indicating the promising activity of CPT/derivatives against resistant mutations, and further support our proposal of this novel mechanism. The studied molecule showed similar binding mechanism to that of the reference drug (Figure 4). Detailed interaction analysis and binding mechanism is explained under section 3.5.

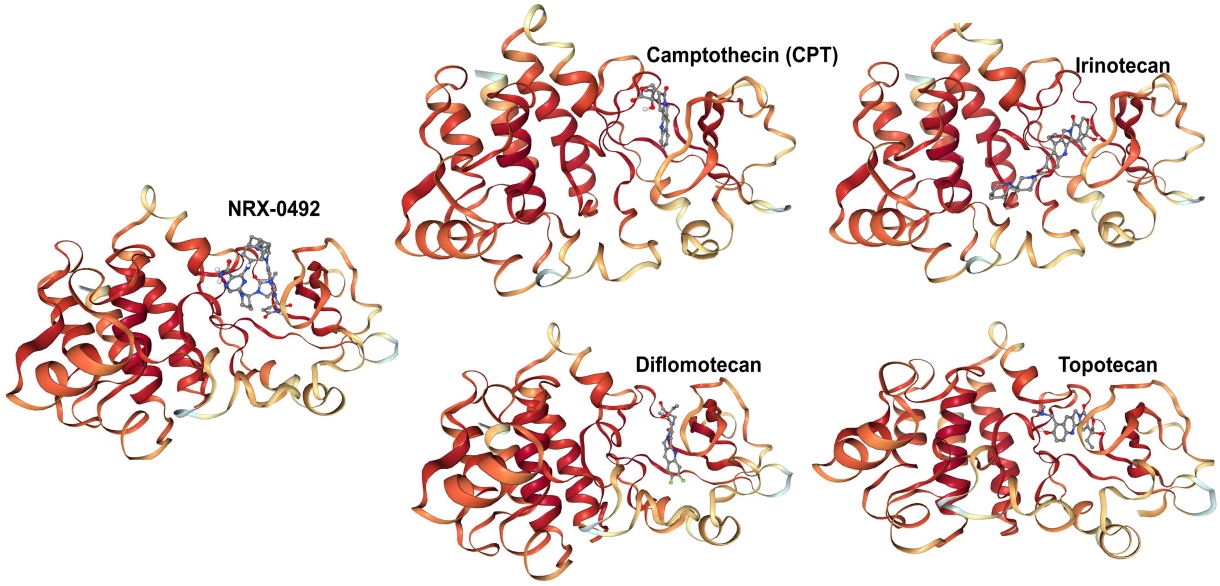

Figure 4. 3D structures of docked complexes of CPT and its derivatives and reference drug (NRX-0492) in the active site pocket of BTK. BTK represented as ribbons and the ligand molecules as ball and stick.

Detailed interaction analysis and binding mechanism of CPT/derivatives are presented under section **3.5**. The 3D coordinates of BTK (WT and mutant)-ligand complexes are provided as Supplementary Material S1, D1.

3.4 MD and Stability of Simulated Systems

Since docking presents the complexes in a static state and allows for observation of only one state, MD simulations were performed to include flexibility of the ligand and protein and allow the system to evolve over a broader conformational landscape for a reasonable period of time. This may allow for observation of interesting conformational events. The MD trajectories for the simulated systems were examined to assess the stability of the compounds in the active site of the protein and to see if there is any significant conformational change in the ligand orientation or position. It was evident from the Root Mean Square Deviation (RMSD) (Figure 5) that all systems compounds exhibited stable binding within the active pocket of RTK.

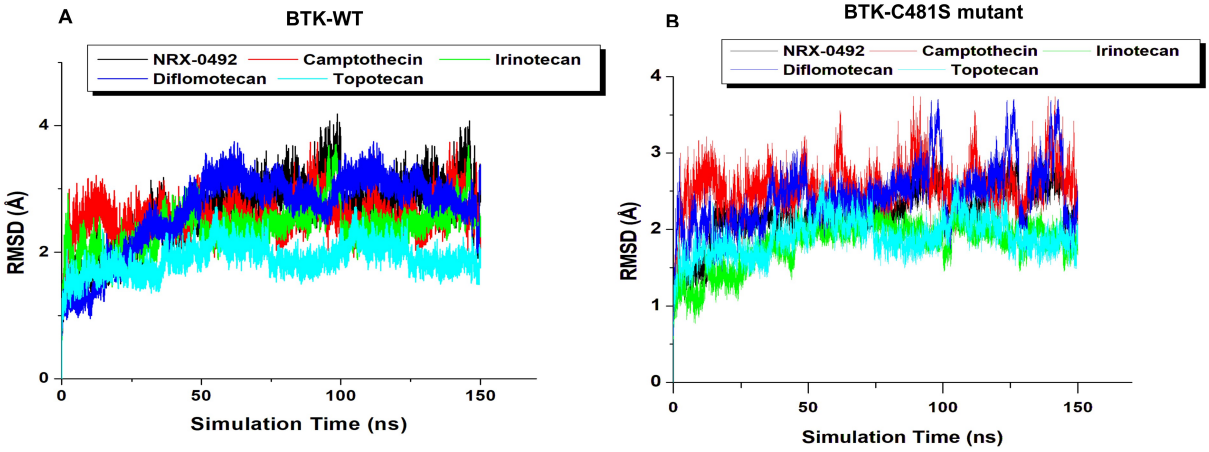

Figure 5: C_α RMSD plots of the ligand-BTK complexes over the MD simulation period; (A) wild type and (B) C481S mutant.

The RMSD fluctuation for all systems remained within 2.5 Å which is a good indication of system stability. We further analysed the MD trajectories at different time interval (50, 100, and 150 ns) to monitor the dynamic interaction pattern between the ligand and protein (Supplementary Material S1, Figure S3). Though all compounds retained residual movements, their poses have not differed significantly from the initial docked poses.

3.5 Interaction Analysis and Binding Mechanism

The MD trajectories for WT and C481S mutant were analyzed and the average structures over 150 ns were collected and presented along with the 2D interaction plots are depicted in Figure 6 and Figure **7**, respectively.

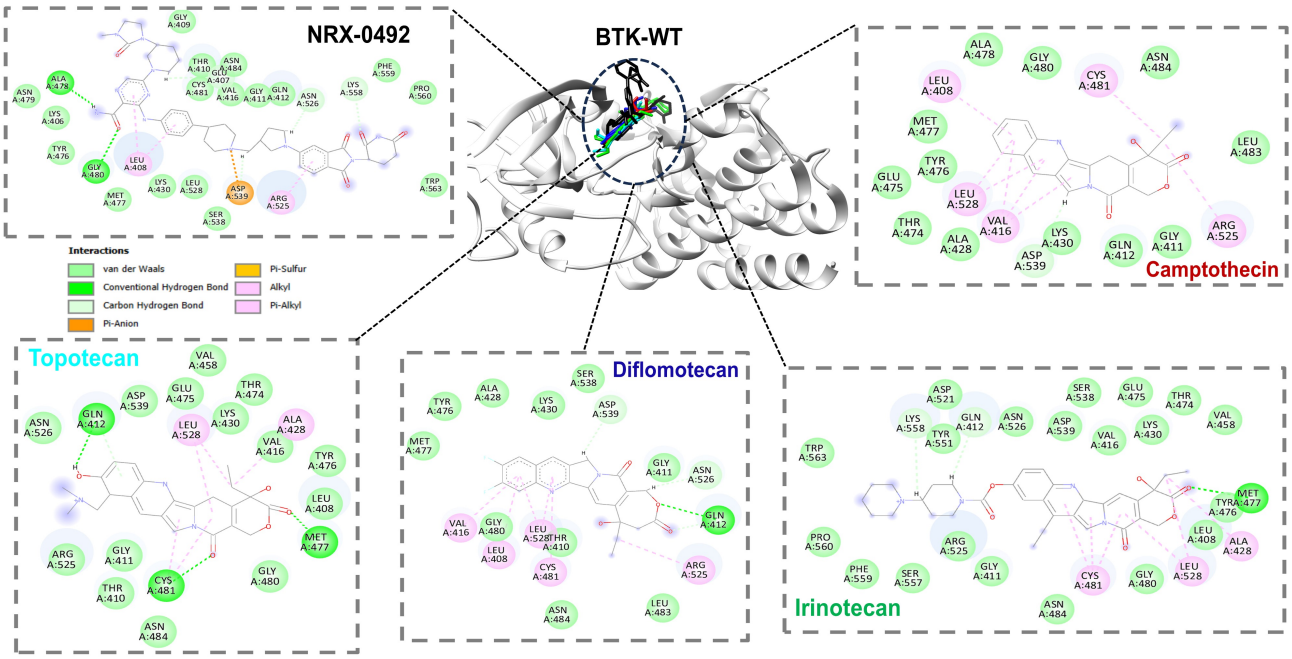

Figure 6. Superimposed 3D structures of ligand-BTK-WT and their 2D interaction plots: CPT (red), Irinotecan (green), Diflomotecan (blue), Topotecan (cyan) and NRX-0492 (black).

Analysis of the WT ligand-protein interactions revealed that, although many conserved interactions were noticed across all studied compounds, there were some variations in the interaction forces. For example, CPT was found to interact with CYS481, ARG525, VAL416, LEU528 and LEU408 via hydrophobic (alkyl/pi-alkyl) interactions. Other weaker interactions such as van der Waals (vdW) were observed with nearby residues in the active site (Figure 6). On the other hand, Irinotecan formed strong hydrogen bonding interaction with MET477, and hydrophobic interactions with ALA428, LEU528 and CYS481, while maintaining weaker vdW interactions with a wider range of nearby residues in the binding site of the protein. This may be due to the fact that the structure of Irinotecan is relatively bigger and has more flexible bonds than CPT and other derivatives, resulting in enhanced binding profile with the protein active site pocket. For Diflomotecan, hydrogen bonding interaction was observed with GLN412, and hydrophobic interactions with ARG525, CYS481, LEU528, LEU408 and VAL416. Topotecan formed hydrogen bond interactions with GLN412 and CYS481, and hydrophobic interactions with ALA428 and LEU528. The reference drug, NRX-0492 showed overall similar interactions as the CPT/derivatives, however, a unique pi-sulfur interaction with ASP539 was observed throughout the MD simulation period. NRX-0492 also formed hydrogen bonding interaction with ALA478 and GLY480, as well as hydrophobic interactions with LEU408 and ARG525. Weaker interactions were observed though with CYS481 and other nearby residues. This may explain that NRX-0492 is active against WT and C481S mutant, since the presence or absence of CYS481 didn't significantly affect its binding affinity, albeit being slightly decreased.

Interestingly, with the C481S mutant (Figure 7), all compounds, with exception of CPT, showed weaker interactions with SER481 than with CYS481 (WT). CPT didn't show interactions with SER481 during the entire simulation time. This may explain the reason why the inhibitory activity of the studied compounds dropped upon mutation. However, despite such decrease in the binding affinity due to the mutation, all compounds retained strong binding, with Irinotecan again exhibiting comparable activity as the reference drug, NRX-0492. Considering that NRX-0492 is known BTK degrader against WT and mutant, we hypothesize that CPT and its derivatives, particularly Irinotecan, could be a strong candidate for further experimental evaluation against the mutant strains.

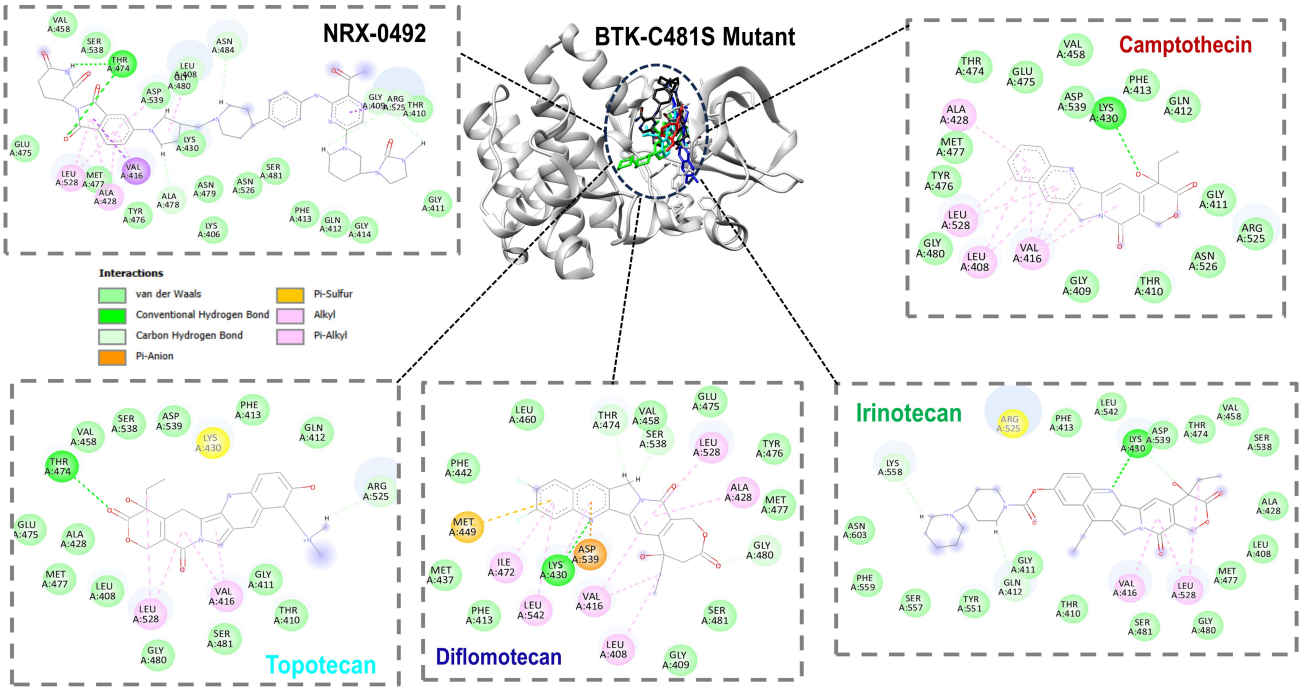

Figure 7. Superimposed 3D structures of ligand-BTK-C481 mutant and their 2D interaction plots: CPT (red), Irinotecan (green), Diflomotecan (blue), Topotecan (cyan) and NRX-0492 (black).

3.6. MM/PBSA Binding Free Energy

The binding energies of the compounds were estimated via MM/PBSA thermodynamic calculations [55], which has proven to produce a reliable estimation of relative binding affinities [56]. The estimated MM/PBSA binding energies were decomposed into their components to determine the main interaction forces that govern the binding of CPT and its analogues with BTK protein, WT and C481S mutant (Table 1). The binding energies ($\Delta G_{binding}$) of Camptothecin, Irinotecan, Diflomotecan, and Topotecan are –34.9±4.5, –42.4±5.3, –37.9±3.4, and –36.4±4.1, respectively, compared to –48.8±3.4 kcal/mol for NRX-0492 (Table 1). The binding free energy calculations were found to be consistent with docking calculations (Supplementary Material, Figure S2).

Table 1. Docking and MM/PBSA binding affinity results for CPT/derivatives, NRX-0492 and binders/non-binders against wild type BTK and C481S mutant (*italic*).

Compound Name	Docking Score (kcal/mol)	MM/PBSA Binding Energy Analysis (kcal/mol)*				
		ΔE_{vdW}	ΔE_{ele}	ΔG_{gas}	ΔG_{sol}	$\Delta G_{binding}$
CPT/Derivatives						
Camptothecin	–9.2 *–8.6*	–39.0±3.1 *–35.8±4.1*	–68.0±13.5 *–67.1±12.3*	–106.0±14.2 *–102.9±13.1*	71.1±11.5 *70.2±10.3*	–34.8±3.5 *–32.4±2.9*
Irinotecan	–11.0 *–10.2*	–51.8±4.1 *–52.2±4.1*	–50.6±15.9 *–50.0±11.2*	–100.4±16.7 *–102.2±11.6*	60.4±14.1 *61.3±14.2*	–42.4±2.3 *–40.9±3.1*
Diflomotecan	–9.8 *–9.6*	–41.1±3.4 *–47.8±5.1*	–15.1±6.4 *–14.9±4.2*	–52.2±7.8 *–62.7±5.9*	28.4±5.2 *27.6±3.2*	–37.9±3.4 *–35.1±3.7*
Topotecan	–9.0 *–8.9*	–41.0±3.4 *–43.9±2.8*	–25.9±9.6 *–24.8±6.9*	–61.9±9.7 *–68.7±8.7*	32.5±7.9 *33.9±7.1*	–36.4±4.1 *–34.8±5.2*
NRX-0492	–11.9 *–10.6*	–52.4±2.8 *–46.6±3.9*	–87.9±4.2 *–87.3±3.3*	–140.3±14.4 *–133.9±13.0*	91.5±13.5 *88.1±12.1*	–48.8±3.4 *–45.8±4.3*
Binders						
PubChem91801213	–11.4 *–10.5*	–53.2±2.4 *–53.6±3.4*	–67.1±3.5 *–66.4±3.1*	–120.3±5.7 *–120.0±4.8*	77.8±4.3 *80.0±3.9*	–42.4±4.2 *–40.0±5.0*
PubChem25154877	–10.9 *–9.9*	–49.1±3.3 *–47.9±4.0*	–56.1±6.1 *–55.2±5.0*	–105.3±7.1 *–103.1±7.6*	63.4±3.0 *64.2±3.4*	–41.9±3.4 *–38.9±2.9*
Non-binders						
PubChem16722836	–7.2 *–6.3*	–35.1±3.2 *–35.2±3.0*	–18.3±6.4 *–17.7±6.5*	–53.4±5.2 *–52.9±4.2*	23.6±5.1 *25.2±4.6*	–29.7±2.8 *–27.7±1.9*
PubChem72695751	–8.1 *–7.0*	–34.1±3.0 *–32.6±4.1*	–17.1±4.1 *–16.4±3.9*	–51.2±6.6 *–49.0±5.0*	20.5±5.0 *21.2±3.1*	–30.8±3.0 *–27.8±3.1*

* **ΔE_{vdW}** = van der Waals energy, **ΔE_{ele}** = Electrostatic energy, **ΔG_{gas}** = gas phase free energy, and **ΔG_{sol}** = solvation-free energy.

Comparing the results to those of the binders, non-binders and reference drug (Table 1), CPT and its derivatives could be potential BTK inhibitors, with Irinotecan being the most active derivative, with ~ 6 kcal/mol binding energy difference from the reference drug, NRX-0492.

With exception of Irinotecan, the relatively lower binding affinity of CPT, Diflomotecan and Topotecan when compared to NRX-0492 may be attributed to the fact these compounds are smaller and flatter. Flat structures are often less flexible, don't allow for a wider range of interactions with amino acid residues in the binding pocket. Irinotecan demonstrated higher binding affinity than CPT and the other analogues, and this again may be explained on the basis that Irinotecan has more flexible structure than the other analogues, which might lead to better interactions with a larger number of amino acid residues in the binding pocket. This may also explain why NRX-0492 has a higher binding affinity, given the flexibility of its structure.

3.7 Key Pharmacophoric Features of CPT/derivatives and Perspective on Structure Activity Relationship (SAR)

To obtain further insight into the structure activity relationship (SAR) of the studied compounds, we mapped the key pharmacophoric features based on the interactions between the ligands and the amino acid residues in the active site (Figure 8). The ligand-BTK complexes were uploaded to Zincpharmer (http://zincpharmer.csb.pitt.edu/) and the pharmacophoric moieties were automatically created based on the interactions between the ligands and the protein receptor.

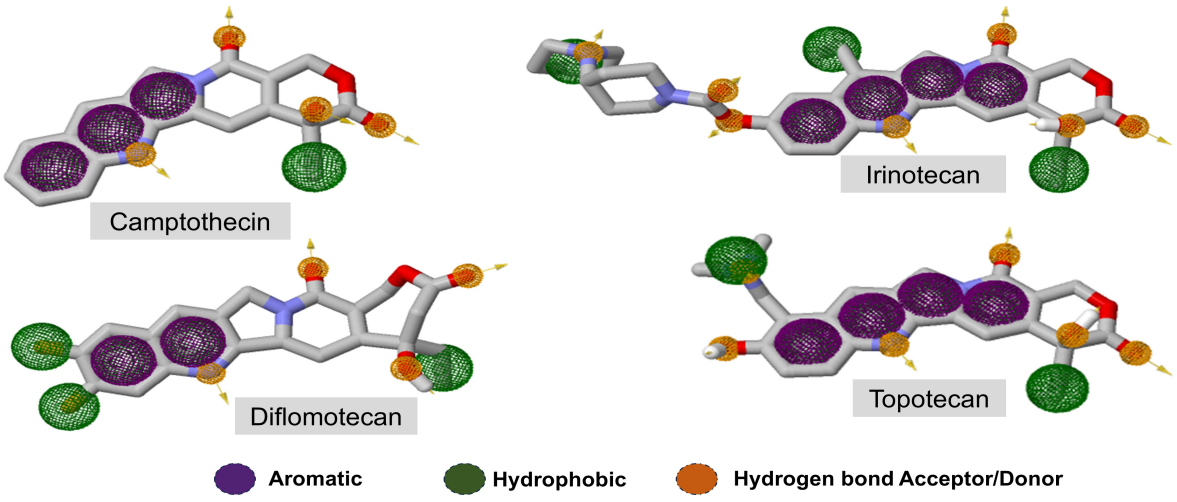

Figure 8. The pharmacophoric features and key interacting groups of CPT/derivatives with the BTK protein. The protein structure was removed for clarity.

As can be seen from Figure 8 that all compounds share a common key pharmacophoric features, however, Irinotecan exhibited a wider range of interacting pharmacophoric groups (3 hydrophobic interactions) when compared to the rest of the compounds. This may explain the superior binding affinity of Irinotecan. Diflomotecan showed 3 hydrophobic pharmacophore groups which may explain its promising binding affinity when compared to CPT and Topotecan. It can be concluded that hydrophobic interactions play a major role in governing the binding interactions of CPT and its derivatives with BTK. To Further confirm this, we mapped the hydrophobic profile of the active site of the BTK (Figure 9)..

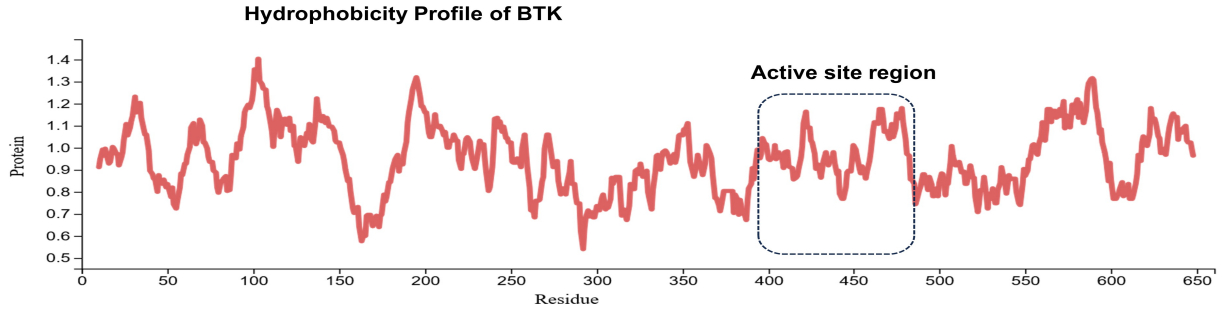

Figure 9. The hydrophobicity profile of BTK protein showing the active site region (dotted rectangle).

It can be observed from Figure 9 that the active site residues are mainly hydrophobic in nature which may explain that hydrophobic interactions are the main driving binding force between CPT/derivatives and BTK

4. Conclusions

Long recognized for their anti-cancer properties, Camptothecin (CPT) and its derivatives (Irinotecan, Diflomotecan, and Topotecan) from Traditional Chinese Medicine (TCM) have been backed by several clinical trials. Topoisomerase I (Topo I) inhibition is the commonly reported mechanism of their anti-cancer effect. There is a lack of research on other possible mechanisms of action of CPT and its analogues. In this study, we proposed that CPT and its analogues could be putative inhibitors of BTK. The potential inhibitory mechanism of CPT/derivatives against BTK was investigated using molecular docking and dynamics simulations coupled with binding free energy calculations. NRX-0492, an orally active wild/mutant-BTK inhibitor, was used as a reference drug to make a rational comparison of the binding mechanism of CPT and its analogues. In order to examine how a mutation affects ligand binding and determine whether CPT or its derivatives can effectively combat drug-resistant mutations, the C481S mutation was also taken into consideration. MD simulations demonstrated stable binding interactions between CPT/analogues and BTK protein throughout the 150 ns simulation time. Similar interaction pattern was observed across all studied compounds. Binding affinity analysis suggested that CPT and its analogues could potentially bind to BTK comparably to NRX-0492. Irinotecan exhibited the highest binding affinity of $\Delta G_{binding}$ = –42.4 kcal/mol, comparable to NRX-0492 ($\Delta G_{binding}$ = –48.8 kcal/mol). This may be due to the relatively bigger structure and flexibility of Irinotecan when compared to other analogues. Irinotecan also showed wider range of pharmacophoric groups interacting with the active site residues of BTK. Despite a minor reduction in binding affinity due to the C481S mutation, the investigated drugs shown promising effectiveness against the mutant.

Despite being a computational study, the results may provide the groundwork for additional experimental research into the as-yet-undiscovered putative anti-cancer mechanism of CPT/derivatives and present a fresh angle on the repurposing of natural products in cancer therapy.

Acknowledgement

The authors would like to thank the Centre for High-Performance Computing (CHPC) (www.chpc.ac.za), Cape Town, South Africa, for the computational resources.

Conflict of Interest

The authors have no conflicts of interest to disclose, both financially and intellectually.

Ethics Approval and Consent to Participate

There were no animals used throughout this research.

Consent to Participate

Not Applicable

Consent to Publication

All authors have approved the publication of the manuscript.

Availability of Data and Material

Not Applicable

Code Availability

Not Applicable

Author Contributions

MS: Conceptualization and research design, final revision, editing, corrections; AI: data collection, experimental, data analysis, drafting manuscript. All authors approved publication.

References

[1] Newman DJ, Cragg GM. Natural Products as Sources of New Drugs over the Nearly Four Decades from 01/1981 to 09/2019. Journal of Natural Products. 2020, 83(3), 770–803.

[2] Li F, Jiang T, Li Q, Ling X. Camptothecin (CPT) and its derivatives are known to target topoisomerase I (Top1) as their mechanism of action: did we miss something in CPT analogue molecular targets for treating human disease such as cancer? American Journal of Cancer Research. 2017, 7(12), 2350-2394.

[3] Moertel CG, Schutt AJ, Reitemeier RJ, Hahn RG. Phase II study of camptothecin (NSC-100880) in the treatment of advanced gastrointestinal cancer. Cancer Chemotherapy Reports. 1972, 56(1), 95-101.

[4] Gottlieb JA, Guarino AM, Call JB, Oliverio VT, Block JB. Preliminary pharmacologic and clinical evaluation of camptothecin sodium (NSC-100880). Cancer Chemotherapy Reports. 1970, 54(6), 461-70.

[5] Cao J, Qi F, Liu T. Adjuvant chemotherapy after curative resection for gastric cancer: A meta-analysis. Scandinavian Journal of Gastroenterology. 2014, 49, 690-704.

[6] Almeida A, Fernandes E, Sarmento B, Lúcio M. A Biophysical Insight of Camptothecin Biodistribution: Towards a Molecular Understanding of Its Pharmacokinetic Issues. Pharmaceutics. 2021, 13(6), 869.

[7] Liu LF, Desai SD, Li TK, Mao Y, Sun M, et al. Mechanism of action of camptothecin. Annals of the New York Academy of Sciences. 2000, 922, 1-10.

[8] Legarza K, Yang LX. The Binding Site of the Cleavable Complex New Molecular Mechanisms of Action of Camptothecin-type Drugs. Anticancer Research. 2006, 26(5A), 3301-5.

[9] Abelson HT, Penman S. Selective interruption of high molecular weight RNA synthesis in HeLa cells by

camptothecin. Nature Cell Biology. 1972, 237(74), 144-6.
[10] Kessel D. Effects of camptothecin on RNA synthesis in leukemia L1210 cells. Biochimica et Biophysica Acta (BBA). 1971, 246(2), 225-32.
[11] Liu YQ, Li WQ, Morris-Natschke SL, Qian K, Yang L, et al. Perspectives on biologically active camptothecin derivatives. Medicinal Research Reviews. 2015, 35(4), 753-789.
[12] Heng Y, Liang Y, Zhang J, Li L, Zhang W, et al. Camptothecin Inhibits Neddylation to Activate the Protective Autophagy Through NF- κ B/AMPK/mTOR/ULK1 Axis in Human Esophageal Cancer Cells. Frontiers in Oncology. 2021, 11, 671180.
[13] Pommier Y. Topoisomerase I inhibitors: camptothecins and beyond. Nat Rev Cancer. 2006, 6(10), 789-802.
[14] Mabb AM, Simon JM, King IF, Lee HM, An LK, et al. Topoisomerase 1 Regulates Gene Expression in Neurons through Cleavage Complex-Dependent and -Independent Mechanisms. PLoS One. 2016, 11(5), e0156439.
[15] Roskoski RJ. A historical overview of protein kinases and their targeted small molecule inhibitors. Pharmacological Research. 2015, 100, 1-23.
[16] Gross S, Rahal R, Stransky N, Lengauer C, Hoeflich KP. Targeting cancer with kinase inhibitors. Journal of Clinical Investigation. 2015, 125(5), 1780-1789.
[17] Hanahan D, Weinberg RA. Hallmarks of cancer: the next generation. Cell. 2011, 144(5), 646-74.
[18] Rip J, Van Der Ploeg EK, Hendriks RW, Corneth OBJ. The Role of Bruton's Tyrosine Kinase in Immune Cell Signaling and Systemic Autoimmunity. Critical Reviews™ in Immunology. 2018, 38(1), 17-62.
[19] Rip J, de Bruijn MJW, Appelman MK, Pal Singh S, Hendriks RW, et al. Toll-Like Receptor Signaling Drives Btk-Mediated Autoimmune Disease. Frontiers in Immunology. 2019, 10, 95.
[20] Di Liberto V, Mudò G, Belluardo N. Crosstalk between receptor tyrosine kinases (RTKs) and G protein-coupled receptors (GPCR) in the brain: Focus on heteroreceptor complexes and related functional neurotrophic effects. Neuropharmacology. 2019, 152, 67-77.
[21] Liu J, Guiadeen D, Krikorian A, Gao X, Wang J, et al. Discovery of 8-Amino-imidazo[1,5-a]pyrazines as Reversible BTK Inhibitors for the Treatment of Rheumatoid Arthritis. ACS Medicinal Chemistry Letters. 2016, 7(2), 198-203.
[22] Pal Singh S, Dammeijer F, Hendriks RW. Role of Bruton's tyrosine kinase in B cells and malignancies. Molecular Cancer. 2018, 17, 57.
[23] Cameron F, Sanford M. Ibrutinib: first global approval. Drugs. 2014, 74(2), 263-71.
[24] Blackmon A, O'Brien S. An update on acalabrutinib to treat chronic lymphocytic leukemia. Drugs Today (Barc). 2021, 57(7), 417-431.
[25] Syed YY. Zanubrutinib: First Approval. Drugs. 2020, 80(1), 91-97.
[26] Schafer PH, Kivitz AJ, Ma J, Korish S, Sutherland D, et al. Spebrutinib (CC-292) Affects Markers of B Cell Activation, Chemotaxis, and Osteoclasts in Patients with Rheumatoid Arthritis: Results from a Mechanistic Study. Rheumatology and Therapy. 2020, 7(1), 101-119.
[27] Gillooly KM, Pulicicchio C, Pattoli MA, Cheng L, Skala S, et al. Bruton's tyrosine kinase inhibitor BMS-986142 in experimental models of rheumatoid arthritis enhances efficacy of agents representing clinical standard-of-care. PLoS One. 2017, 12(7), e0181782.
[28] Narita Y, Nagane M, Mishima K, Terui Y, Arakawa Y, et al. Phase I/II study of tirabrutinib, a second-generation Bruton's tyrosine kinase inhibitor, in relapsed/refractory primary central nervous system lymphoma. Neuro-Oncology. 2021, 23(1), 122-133.
[29] Cohen S, Tuckwell K, Katsumoto TR, Zhao R, Galanter J, et al. Fenebrutinib versus Placebo or Adalimumab in Rheumatoid Arthritis: A Randomized, Double-Blind, Phase II Trial (ANDES Study). Arthritis & Rheumatology. 2020, 72(9), 1435-1446.
[30] Smith PF, Krishnarajah J, Nunn PA, Hill RJ, Karr D, et al. A phase I trial of PRN1008, a novel reversible covalent inhibitor of Bruton's tyrosine kinase, in healthy volunteers. British Journal of Clinical Pharmacology. 2017, 83(11), 2367-2376.
[31] Rozkiewicz D, Hermanowicz JM, Kwiatkowska I, Krupa A, Pawlak D. Bruton's Tyrosine Kinase Inhibitors (BTKIs): Review of Preclinical Studies and Evaluation of Clinical Trials. Molecules. 2023, 28(5), 2400.
[32] Goldwasser F, Shimizu T, Jackman J, O'Connor PM, Kohn KW, et al. Correlations between S and G2 Arrest and the Cytotoxicity of Camptothecin in Human Colon Carcinoma Cells. Cancer Research. 1996, 56(19), 4430-7.
[33] Zhang D, Harris HM, Chen J, Judy J, James G, et al. NRX-0492 degrades wild-type and C481 mutant BTK and demonstrates in vivo activity in CLL patient-derived xenografts. Blood. 2023,141(13), 1584-1596.
[34] Qi J, Endres S, Yosifov DY, Tausch E, Dheenadayalan RP, et al. Acquired BTK mutations associated with resistance to noncovalent BTK inhibitors. Blood Advances. 2023, 7(19), 5698-5702.
[35] Elamin G, Aljoundi A, Alahmdi MI, Abo-Dya NE, Soliman MES. Battling BTK mutants with noncovalent inhibitors that overcome Cys481 and Thr474 mutations in Waldenström macroglobulinemia therapy: structural mechanistic insights on the role of fenebrutinib. Journal of Molecular Modeling. 2022, 28(11), 355.
[36] Pettersen EF, Goddard TD, Huang CC, Couch GS, Greenblatt DM, et al. UCSF Chimera-A visualization system for exploratory research and analysis. Journal of Computational Chemistry. 2004, 25(13), 1605-12.
[37] Cherinka B, Andrews BH, Sánchez-Gallego J, Brownstein J, Argudo-Fernández M, et al. Marvin: A Tool Kit for Streamlined Access and Visualization of the SDSS-IV MaNGA Data Set. The Astronomical Journal. 2019, 158, 74.
[38] Hanwell MD, Curtis DE, Lonie DC, Vandermeersch T, Zurek E, et al. Avogadro: an advanced semantic chemical editor, visualization, and analysis platform. Journal of Cheminformatics. 2012, 4, 17.
[39] Dallakyan S, Olson AJ. Small-molecule library screening by docking with PyRx. Methods in Molecular Biology. 2015, 1263, 243-50.
[40] Trott O, Olson AJ. AutoDock Vina: improving the speed and accuracy of docking with a new scoring function, efficient optimization, and multithreading. Journal of Computational Chemistry. 2010, 31(2), 455-461.
[41] Song LF, Lee TS, Zhu C, York DM, Merz KM. Using AMBER18 for Relative Free Energy Calculations. Journal of Chemical Information and Modeling. 2019, 59(7), 3128-3135.
[42] Maier JA, Martinez C, Kasavajhala K, Wickstrom L, Hauser KE, et al. ff14SB: Improving the Accuracy of Protein Side Chain and Backbone Parameters from ff99SB. Journal of Chemical Theory and Computation. 2015, 11(8), 3696-3713.
[43] Wang J, Wolf RM, Caldwell JW, Kollman PA, Case DA. Development and testing of a general amber force field. Journal of Computational Chemistry. 2004, 25(9), 1157-74.
[44] Bayly CI, Cieplak P, Cornell WD, Kollman PA. A well-behaved electrostatic potential based method using

charge restraints for deriving atomic charges: The RESP model. Journal of Physical Chemistry. 1993, 97(40), 10269-10280.
[45] Wang J, Wang W, Kollman PA, Case DA. Automatic atom type and bond type perception in molecular mechanical calculations. Journal of Molecular Graphics and Modelling. 2006, 25(2), 247-260.
[46] Larini L, Mannella R, Leporini D. Langevin stabilization of molecular-dynamics simulations of polymers by means of quasisymplectic algorithms. The Journal of Chemical Physics. 2007, 126, 104101.
[47] Lin Y, Pan D, Li J, Zhang L, Shao X. Application of Berendsen barostat in dissipative particle dynamics for nonequilibrium dynamic simulation. The Journal of Chemical Physics. 2017, 146(12), 124108.
[48] Gonnet P. P-SHAKE: a quadratically convergent SHAKE in O (n^2). Journal of Computational Physics. 2007, 220(2), 740-750.
[49] Roe DR, Cheatham III TE. PTRAJ and CPPTRAJ: software for processing and analysis of molecular synamics trajectory data. Journal of Chemical Theory and Computation. 2013, 9, 3084-309595.
[50] Agnihotry S, Pathak RK, Singh DB, Tiwari A, Hussain I. Protein structure prediction. Bioinformatics: Methods and Applications. 2021, 177-88.
[51] Mateev E, Valkova I, Angelov B, Georgieva M, Zlatkov A. VALIDATION THROUGH RE-DOCKING, CROSS-DOCKING AND LIGAND ENRICHMENT IN VARIOUS WELL-RESOLUTED MAO-B RECEPTORS. International Journal of Pharmaceutical Sciences and Research. 2022, 13(3), 1099-1107.
[52] Slavov S, Beger RD. Identification of structural factors that affect binding to cannabinoid receptor type 1. Journal of Molecular Structure. 2022, 1249, 131589.
[53] Rajapakse M, Feng L. Predicting Peptide Binders of Flexible Lengths with Genetic Annealing Algorithm. Advanced Materials Research. 2013, 805-806, 1856.
[54] Weiss DR, Karpiak J, Huang XP, Sassano MF, Lyu J, et al. Selectivity Challenges in Docking Screens for GPCR Targets and Antitargets. Journal of Medicinal Chemistry. 2018, 61(15), 6830-6845.
[55] Miller BR, Mcgee TD, Swails JM, Homeyer N, Gohlke H, et al. MMPBSA.py : An E ffi cient Program for End-State Free Energy Calculations. Journal of Chemical Theory and Computation. 2012, 8(9),3314-3321.
[56] Genheden S, Ryde U. The MM/PBSA and MM/GBSA methods to estimate ligand-binding affinities. Expert Opinion on Drug Discovery. 2015, 10(5), 449-461.

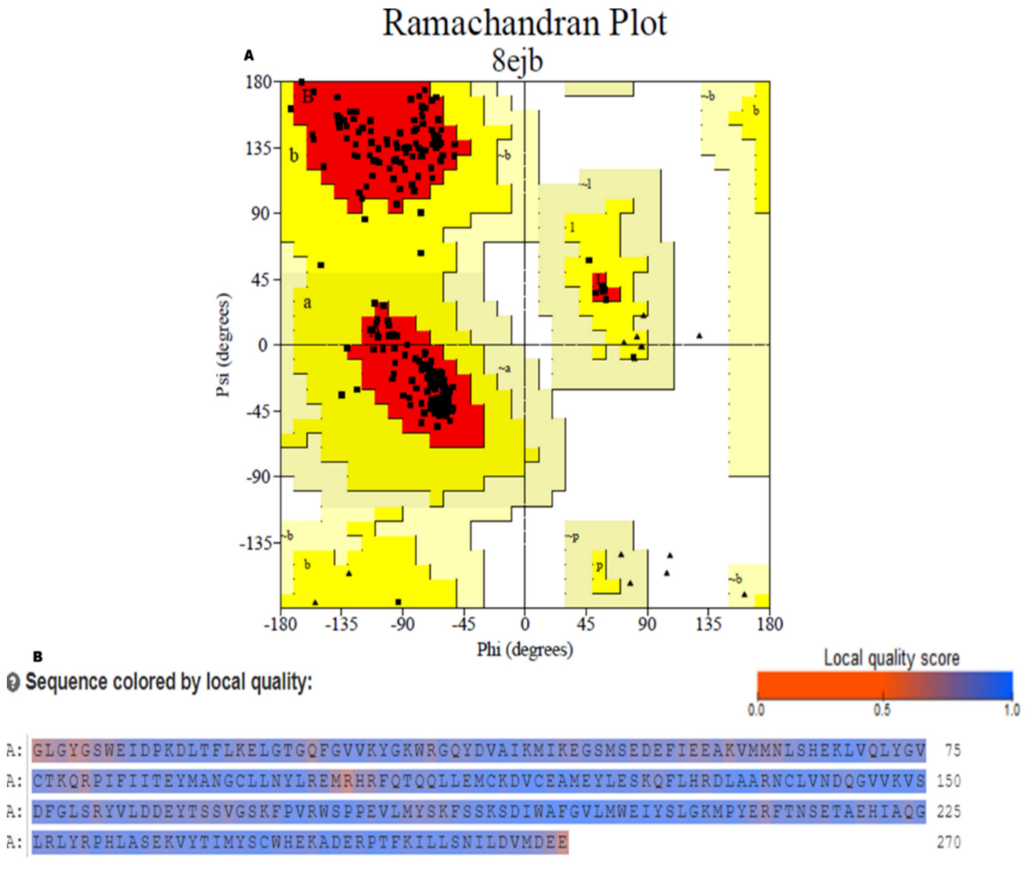

Figure S1. Plots showing the quality of the BTK structure (PDB ID: 8ejb) used for this study. (A) Ramachandran plots, which suggest 95.5% of the residues are within the highly favoured region, and (B) the sequence of the BTK structure coloured by local quality.

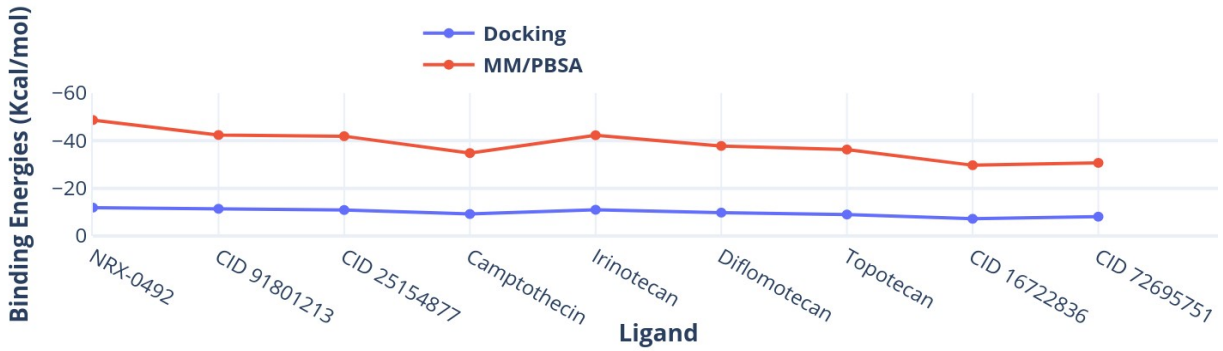

Figure S2. Docking vs. MM/PBSA binding energy results, showing consistency between the docking and binding energy calculations (MM/PBSA).

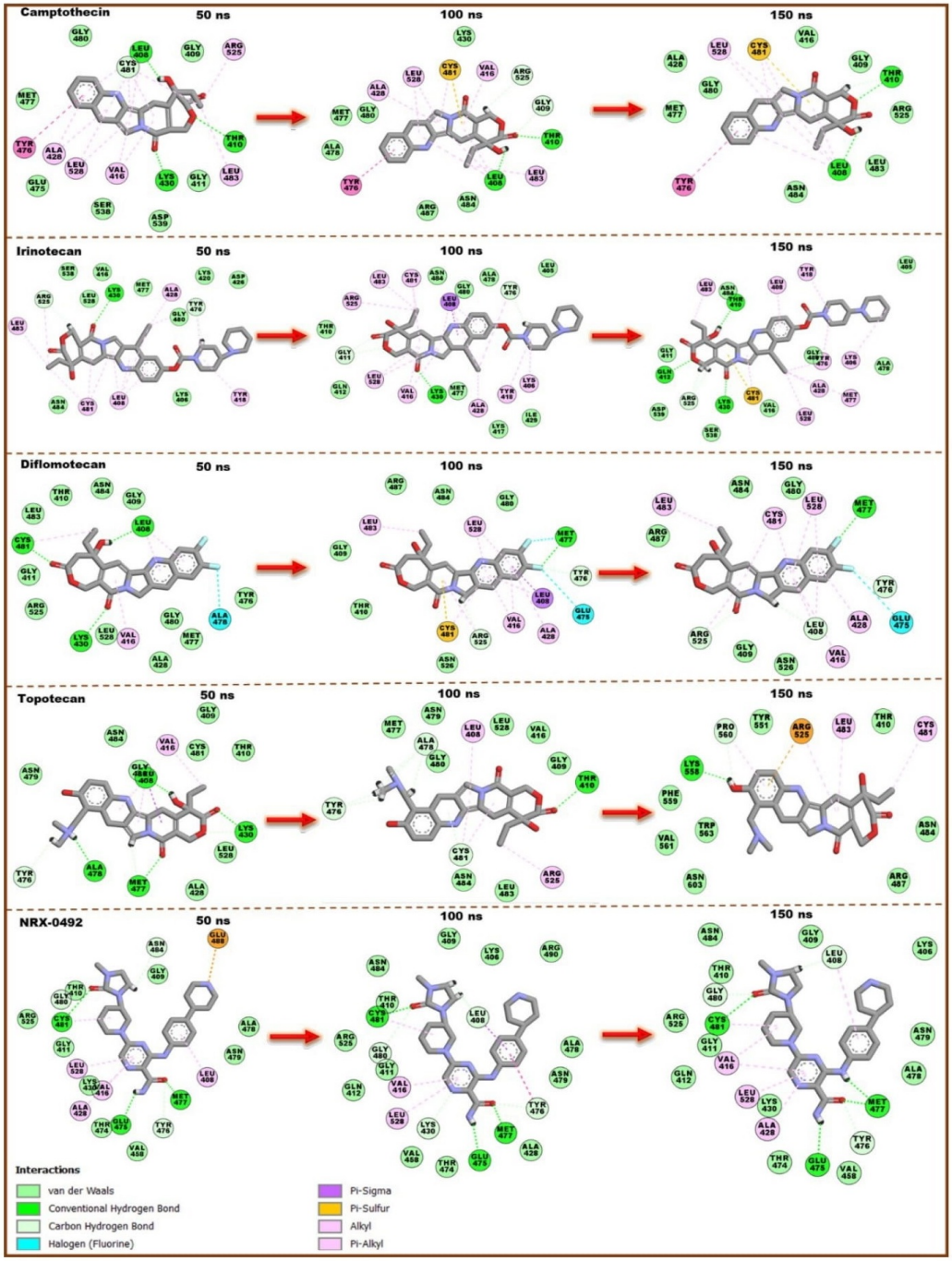

Figure S3. 2D representation of the conformational dynamics of the compounds within the BTK active site. Snapshots are taken at 50, 100, and 150 ns of the MD trajectory